the plant journal

SEB Society for Experimental Biology

The Plant Journal (2019) **98,** 826–841 doi: 10.1111/tpj.14276

In situ transcriptomic and metabolomic study of the loss of photosynthesis in the leaves of mixotrophic plants exploiting fungi

Félix Lallemand[1], Marie-Laure Martin-Magniette[2,3,4], Françoise Gilard[2,5], Bertrand Gakière[2,5], Alexandra Launay-Avon[2,3], Étienne Delannoy[2,3,*] and Marc-André Selosse[1,6]

[1]*Institut de Systématique, Evolution, Biodiversité (ISYEB), Muséum national d'Histoire naturelle, CNRS, Sorbonne Université, EPHE, CP 39, 57 rue Cuvier, 75005 Paris, France,*

[2]*Institute of Plant Sciences Paris-Saclay (IPS2), CNRS, INRA, Université Paris-Sud, Université Evry, Université Paris-Saclay, 91405 Orsay, France,*

[3]*Institute of Plant Sciences Paris-Saclay IPS2, Paris-Diderot, Sorbonne Paris-Cité, 91405 Orsay, France,*

[4]*UMR MIA-Paris, AgroParisTech, INRA, Université Paris-Saclay, Paris, France,*

[5]*Plateforme Métabolisme Métabolome, Institute of Plant Sciences Paris-Saclay (IPS2), CNRS, INRA, Univ. Paris-Sud, Univ. Evry, Univ. Paris-Diderot, Univ. Paris-Saclay, Bâtiment 630 Rue Noetzlin, 91192 Gif-sur-Yvette Cedex, France, and*

[6]*Faculty of Biology, University of Gdańsk, ul. Wita Stwosza 59, 80-308 Gdańsk, Poland*

Received 7 September 2018; revised 31 January 2019; accepted 1 February 2019; published online 8 February 2019.
*For correspondence (e-mail etienne.delannoy@inra.fr).

SUMMARY

Mycoheterotrophic plants have lost photosynthesis and obtain carbon through mycorrhizal fungi colonizing their roots. They are likely to have evolved from mixotrophic ancestors, which rely on both photosynthesis and fungal carbon for their development. Whereas our understanding of the ecological and genomic changes associated with the evolutionary shift to mycoheterotrophy is deepening, little information is known about the specific metabolic and physiological features driving this evolution. We investigated this issue in naturally occurring achlorophyllous variants of temperate mixotrophic orchids. We carried out an integrated transcriptomic and metabolomic analysis of the response to achlorophylly in the leaves of three mixotrophic species sampled *in natura*. Achlorophyllous leaves showed major impairment of their photosynthetic and mineral nutrition functions, strong accumulation of free amino acids, overexpression of enzymes and transporters related to sugars, amino acids and fatty acid catabolism, as well as induction of some autophagy-related and biotic stress genes. Such changes were reminiscent of these reported for variegated leaves and appeared to be symptomatic of a carbon starvation response. Rather than decisive metabolic innovations, we suggest that the evolution towards mycoheterotrophy in orchids is more likely to be reliant on the versatility of plant metabolism and an ability to exploit fungal organic resources, especially amino acids, to replace missing photosynthates.

Keywords: mycorrhiza, mycoheterotrophy, mixotrophy, albinos, orchids, Neottieae, metabolomic, transcriptomic, carbon starvation response.

INTRODUCTION

Most plants are associated with soil fungi, forming a so-called mycorrhizal symbiosis in which fungi provide mineral nutrients (water, N, P and K) in exchange for plant organic carbon (van der Heijden *et al.*, 2015). Unlike the usual mycorrhizal symbiosis, mycoheterotrophic plants get both their mineral nutrients and organic carbon from their mycorrhizal fungi (Merckx, 2013). With more than 500 fully mycoheterotrophic species that have lost chlorophyll and photosynthesis, this remarkable evolutionary inversion of mutualistic mycorrhizal interactions has arisen independently at least 50 times, in 17 plant families (Merckx *et al.*, 2013a; Těšitel *et al.*, 2018). However, we have yet to understand the metabolic evolution to mycoheterotrophy (Selosse *et al.*, 2017).

In addition to full mycoheterotrophs, some green plants obtain their carbon by adding photosynthesis and partial mycoheterotrophy in a strategy called mixotrophy (Selosse and Roy, 2009; Těšitel *et al.*, 2018). Orchids have complex

© 2019 The Authors
The Plant Journal © 2019 John Wiley & Sons Ltd

links with mycoheterotrophy and mixotrophy (Bidartondo *et al.*, 2004; Selosse *et al.*, 2004; Roy *et al.*, 2013). All orchids produce reserveless seeds that support their germination and early growth by an initial mycoheterotrophy, thanks to fungi that later become mycorrhizal partners in their roots (Dearnaley *et al.*, 2016). Most species associate with rhizoctonias (a polyphyletic group of fungi; Smith and Read, 2008; Dearnaley *et al.*, 2012), and develop photosynthetic organs that allow autotrophy at adulthood (although their exact level of dependency on fungal carbon is debated; Selosse and Martos, 2014). Some species remain mycoheterotrophic or form green leaves but are mixotrophic at adulthood (Selosse and Roy, 2009). In temperate regions, these orchids do not associate with rhizoctonias but with ecologically and taxonomically different fungi that simultaneously form symbioses with surrounding tree roots called ectomycorrhizas (Julou *et al.*, 2005; Waterman *et al.*, 2013). Mixotrophic orchids are phylogenetically close to mycoheterotrophic species, and mixotrophy is therefore considered an evolutionary step towards full mycoheterotrophy. Mixotrophy represents a unique model to understand how mycoheterotrophy has evolved (Selosse and Roy, 2009).

Rare but compelling field evidence that mixotrophy is a step in the evolution to mycoheterotrophy has been seen through observation in some mixotrophic orchids that are normally green of individuals fully devoid of chlorophyll (Selosse *et al.*, 2004; Julou *et al.*, 2005). These 'albinos' survive well (Salmia, 1989; Shefferson *et al.*, 2016) but produce fewer seeds (Roy *et al.*, 2013). They especially occur in the closely related genera *Epipactis* (Selosse *et al.*, 2004; Gonneau *et al.*, 2014; Lewis, 2015) and *Cephalanthera* (Julou *et al.*, 2005; Abadie *et al.*, 2006; Sakamoto *et al.*, 2016).

Our understanding of mixotrophic physiology remains limited. Most studies have relied on natural stable isotopes as a proxy for the level of mycoheterotrophy, as the organic matter gained from fungi is naturally enriched in ^{13}C compared with that obtained by photosynthesis (see Hynson *et al.* (2013) for a review). This allows calculation of the percentage of carbon recovered from mycorrhizal fungi in a given organ at a given stage (e.g., Roy *et al.*, 2013; Gonneau *et al.*, 2014). The level of mycoheterotrophy depends on species and environmental conditions and decreases with increasing light availability (Preiss *et al.*, 2010; Gonneau *et al.*, 2014; Lallemand *et al.*, 2017) and during the growth season, as expected from the development of green leaves (Roy *et al.*, 2013; Gonneau *et al.*, 2014). Isotopic analysis, however, does not give access to metabolism in mixotrophs or especially in albinos, which mimic the emergence of mycoheterotrophy.

In a pioneer study, Suetsugu *et al.* (2017) compared the differences in gene expression in mycorrhizal roots between green and albino individuals of the mixotrophic *Epipactis helleborine* (L.) Crantz. Surprisingly, gene expression displayed rather little alteration in either the plant or the fungi in this symbiotic organ. Both roots and fungi showed upregulation of genes related to antioxidant function, possibly reflecting a higher lysis of hyphae in mycorrhizas. Both partners also exhibited a higher expression of genes encoding nutrient transporters, such as a bidirectional sugar transporter SWEET or transporters from the 'major facilitator' superfamily involved in the exchange of various nutrients (Pao *et al.*, 1998), organic (e.g. sugars, nucleosides and amino acids) and inorganic (e.g. nitrates, phosphates). The minor changes found mycorrhizas due to such a dramatic loss of photosynthesis call for further investigation in other organs, especially in leaves in which metabolism may be more affected by albinism. Moreover, metabolite abundance is valuable data for interpreting changes in gene expression, calling for biochemical investigations of the mycoheterotrophic albino lifestyle.

Here, we report a multiomics, multipopulation and multispecies analysis comparing the leaf transcriptome and metabolome of albino and green individuals in mixotrophic orchids. By combining transcriptomic and metabolomic profiling of albinos in three species (*Cephalanthera damasonium* (Mill) Druce, *E. helleborine* and *E. purpurata* Sm.) collected *in situ* from different populations, we aimed to filter RNA and biochemical variability due to species-specific or environment-specific features. This approach allowed us to focus on the potential core physiological changes associated with mixotrophy and related to the shift towards full mycoheterotrophy. We discuss these results with regard to the evolution of mixotrophy and mycoheterotrophy in orchids.

RESULTS

The response to albinism is globally shared by the three species

In total, 156 compounds, shared by all the samples, corresponding to 141 different metabolites, were identified by GC-MS analysis (Table S1). This included most of the compounds from primary metabolism (see Table S1 for exceptions). Thirty-three metabolites showed an overaccumulation in albinos compared with green counterparts, whereas 19 were less abundant (Figure 1; Table S1). No metabolite statistically differed in its response to albinism between two species.

RNA-seq analysis showed that 3060 genes (out of 14 845 after filtering out genes with low expression) were differentially expressed between albinos and green counterparts (Data S1). When only plastid-encoded genes were considered, albinos and green counterparts clustered in two distinctive groups after principal component analysis (PCA) (Figure S1). The distinction was less obvious, but nevertheless present, when considering nuclear-encoded genes: the

© 2019 The Authors
The Plant Journal © 2019 John Wiley & Sons Ltd,

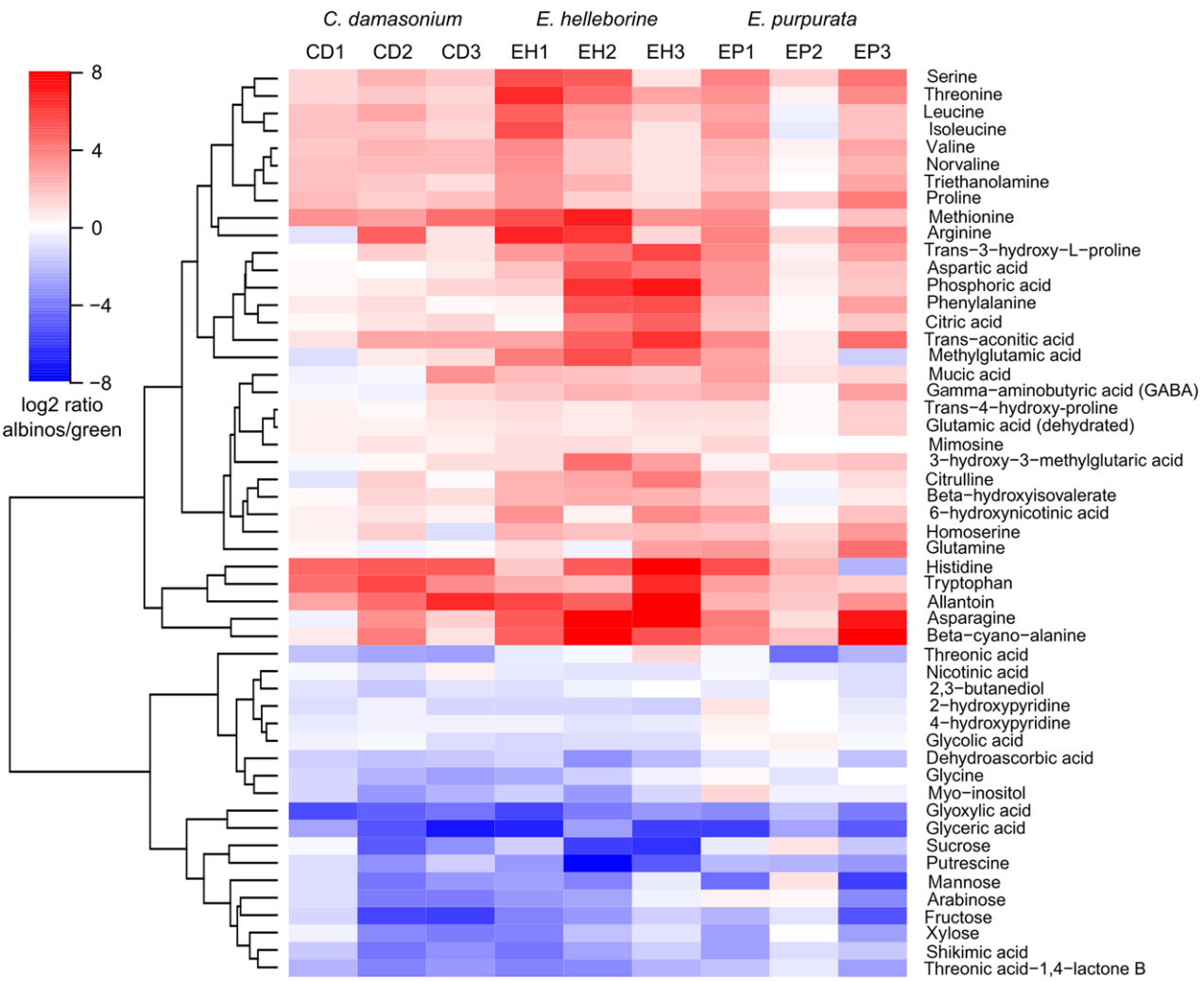

Figure 1. Metabolite abundance differences between albino and green leaves of the three orchid species studied based on GC-MS analysis. Each column corresponded to an albino/green pair (see Table 2 for correspondence with sampling sites). Only metabolites with significant differences are shown (see Table S1 for FDR and fold changes). Red (respectively blue) indicates higher (respectively lower) abundance in albinos compared with green individuals. A hierarchical clustering by the complete linkage method is shown on the left.

distances between individuals of same phenotype roughly equalled the distances between those within an albino/green pair (Figure S1), suggesting that variability among populations and albinism affected gene expression to a similar extent. The same was true for metabolomic data (Figure S1). For *C. damasonium* (CD), individuals from the same site (CD2 and CD3, Boigneville) did not cluster together, indicating high intra-population variability and making these suitable biological replicates (Figure S1). When comparing response to albinism in the three species, intraspecific variability equalled interspecific variability (Figure S1), and we detected only a limited number of genes and no metabolite that statistically differed in response to albinism between the two species (329 genes for comparison between CD and *E. helleborine* (EH) but only 3, 25 and 6 when comparing *E. purpurata* (EP) to CD, EP to EH, or CD to the two *Epipactis*, respectively). This difference is probably caused by the statistical power associated with the low number of replicates per species as well as microenvironmental variations of these field samples, but it nevertheless suggests a conserved response to albinism in all populations for gene expression and metabolite abundance.

Shutdown of photosynthesis-related and mineral nutrition functions

Many genes involved in photosynthesis were repressed in albinos (Figure 2), e.g. nuclear-encoded components of the photosynthetic electron transport chain, enzymes of chlorophyll biosynthesis, the Calvin cycle, photorespiration and plastidial carbonic anhydrase (Data S1). The plastidial genome expression was inhibited but still present in

© 2019 The Authors

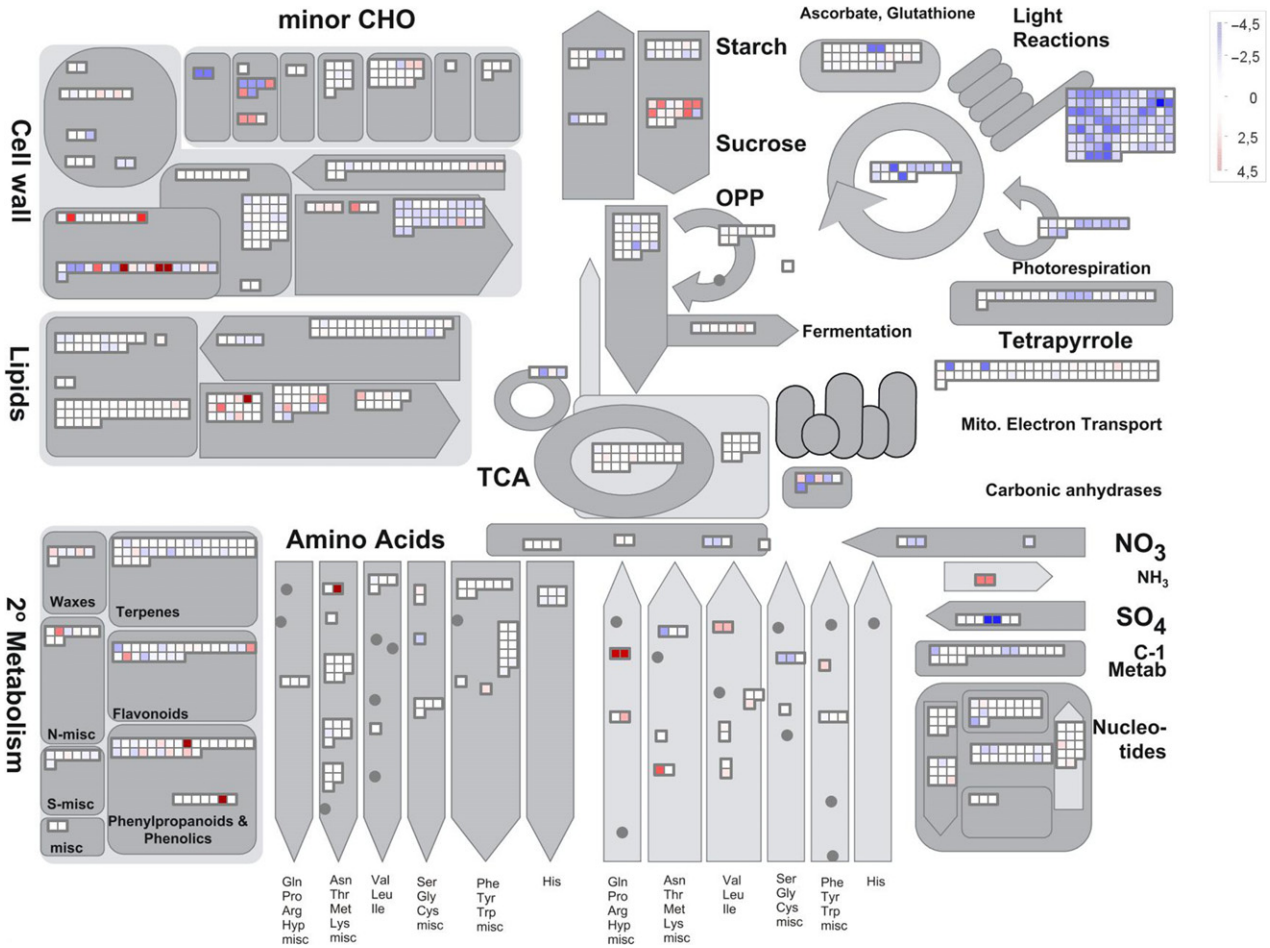

Figure 2. Overview of the average changes in the leave transcriptome of albinos compared with green individuals. In this summary of the plant primary metabolism, drawn with Mapman software (Thimm *et al.*, 2004), each square represents a gene. Based on mean $\log_2$ ratio of the nine albino/green pairs studied, repressed genes are in blue and induced ones in red. See text and Table 1 for gene names and fold changes. CHO, carbohydrates; OPP, oxidative pentose phosphate pathway; TCA, tricarboxylic acid cycle.

albinos with plastidial reads representing 52 ± 10% (mean ± 95% confidence interval) of the total library (compared with 83 ± 5% in green). Within the overall inhibition, plastidial genes transcribed by plastid-encoded RNA polymerase were more strongly inhibited than plastidial genes transcribed by nuclear-encoded RNA polymerase. Decrease in abundance of metabolic intermediates confirms this for photorespiration, but not for the Calvin cycle, in which only 3-phosphoglycerate was detected and did not differ between green and albinos (Table S1). The inability of albinos to photosynthesize, verified by transcriptomic analysis, confirms their mycoheterotrophy.

In association with the photosynthesis shutdown, transporters involved in mineral nutrient translocation were repressed in albinos for nitrate (*NRT2.3*, *NPF6.2*; see Table 1 for detailed names and fold changes), phosphate (*PHO1-H1*, *PHT2-1*), sulfate (*SULTR3.1*, *SULTR3.3*), magnesium (*MRS2-3*, although *MRS2-10* was induced) and zinc (*ZIP2*). Mineral nitrogen assimilation was inhibited in albinos, as shown by repression of ferredoxin-dependent glutamate synthase (*GLU*, but not the NADH-dependent glutamate synthase *GLT1*) and glutamine synthetase (*GLNA4_PHAVU*, Table 1). Sulfate assimilation through cysteine biosynthesis was also strongly reduced in albinos (*APR3*, Table 1).

Major alterations of nitrogen metabolism

Metabolomic analysis revealed a striking increase in abundance of amino acids and their derivatives in albinos compared with green counterparts (Figures 1 and 3; Table S1). The largest increases were for asparagine (24×), histidine (16×), methionine (12×), tryptophan (11×) and arginine (9×), whereas no difference were found for glutamate, alanine, tyrosine and lysine (Table S1). Only glycine was less abundant in albinos (2×), probably due to the low photorespiration revealed from gene expression (Table S1; Data S1). The nitrogen-rich compound allantoin was 23× more abundant in albinos, while the polyamine putrescine

© 2019 The Authors
The Plant Journal © 2019 John Wiley & Sons Ltd,

Table 1 List of the differentially expressed genes involved in major biological processes, which are reported in the main text. Fold changes are the mean log_2 ratio of the nine albino/green pairs studied. When positive (respectively negative), genes are more (less) expressed in albino leaves. Compound names, gene names and enzyme commission (EC) numbers associated with each best blastP, were retrieved from the UniProt database

Biological process	Subcategory	Compound[a]	blastP	Gene name	log_2 ratio
Mineral nutrients	Magnesium	Magnesium transporter MRS2-10	MRS2A_ARATH	MRS2-10	0.76
		Magnesium transporter MRS2-3	MRS23_ARATH	MRS2-3	−1.44
	Nitrate	Protein NRT1/PTR FAMILY 6.2	PTR27_ARATH	NPF6.2	−1.97
		High-affinity nitrate transporter 2.3	NRT23_ORYSJ	NRT2.3	−0.99
	Phosphate	Phosphate transporter PHO1 homolog 1	PHO11_ARATH	PHO1-H1	−3.22
		Inorganic phosphate transporter 2-1, chloroplastic	PHT21_ARATH	PHT2-1	−0.81
	Sulfate	Sulfate transporter 3.1	SUT31_ARATH	SULTR3;1	−2
		Probable sulfate transporter 3.3	SUT33_ARATH	SULTR3;3	−1.85
	Zinc	Zinc transporter 2	ZIP2_ORYSJ	ZIP2	−1.23
Nitrogen metabolism		Asparagine synthetase [glutamine-hydrolyzing]	ASNS_ASPOF		3.5
		Glutamine synthetase leaf isozyme, chloroplastic	GLNA4_PHAVU		−1.71
		Probable isoaspartyl peptidase/L-asparaginase 2	ASPGB_ARATH		−3
		Ferredoxin-dependent glutamate synthase, chloroplastic	GLTB_ORYSJ	GLU	−0.92
Amino acids biosynthesis	Cys	5′-adenylylsulfate reductase 3, chloroplastic	APR3_ARATH	APR3	−3.52
		Cysteine synthase	CYSK2_ORYSJ	RCS3	−1.11
	Val, Ile, Leu	Branched-chain amino acid aminotransferase 3, chloroplastic[b]	BCAT3_ARATH	BCAT3	2.22
		3-isopropylmalate dehydratase large subunit, chloroplastic	LEUC_ARATH	IIL1	−0.71
		2-isopropylmalate synthase A	LEU1A_SOLPN	IPMSA	−2.75
Sugar metabolism	Sucrose	Beta-fructofuranosidase, insoluble isoenzyme 3	INV3_ORYSJ	CIN3	0.84
		Beta-fructofuranosidase 1	INV1_MAIZE	IVR1	1.65
		Neutral/alkaline invertase 1, mitochondrial	NIN1_ORYSJ	NIN1	1.65
		Sucrose-phosphate synthase	SPSA_MAIZE	SPS	−1.6
	Trehalose	Probable trehalase	TRE_ORYSJ		1.47
		Probable trehalose-phosphate phosphatase 2	TPP2_ORYSJ	TPP2	2.28
		Probable trehalose-phosphate phosphatase 6	TPP6_ORYSJ	TPP6	−2
		Alpha,alpha-trehalose-phosphate synthase [UDP-forming] 5	TPS5_ARATH	TPS5	2.4
		Alpha,alpha-trehalose-phosphate synthase [UDP-forming] 6	TPS6_ARATH	TPS6	0.78
		Alpha,alpha-trehalose-phosphate synthase [UDP-forming] 6	TPS6_ARATH	TPS6	1.02
		Probable alpha,alpha-trehalose-phosphate synthase [UDP-forming] 9	TPS9_ARATH	TPS9	1.97
Organic nutrients	Sugars	Sugar transporter ERD6-like 6	ERDL6_ARATH		1.61
		Sugar transport protein 13	STP13_ARATH	STP13	1.36
		Sucrose transport protein SUT1	SUT1_ORYSJ	SUT1	1.5
		Sucrose transport protein SUT2	SUT2_ORYSI	SUT2	−0.78
		Bidirectional sugar transporter SWEET2a	SWT2A_ORYSJ	SWEET2A	1.31
	Amino acids	Probable proline transporter 2	PROT2_ORYSJ		1.03
		Probable amino acid permease 7	AAP7_ARATH	AAP7	1.09
		Lysine histidine transporter-like 8	LHTL8_ARATH	AATL1	1.02
		Amino acid permease BAT1 homolog	BAT1_ORYSJ	BAT1	1.1
Amino acids catabolism	Arg	Ornithine aminotransferase, mitochondrial	OAT_ORYSJ	OAT	1.44
	Lys	Alpha-aminoadipic semialdehyde synthase	AASS_ARATH	LKR/SDH	2.44
	Pro	Proline dehydrogenase 2, mitochondrial	PROD2_ARATH	POX2	2.1
	Tyr	Homogentisate 1,2-dioxygenase	HGD_ARATH	HGO	1.13
		4-hydroxyphenylpyruvate dioxygenase	HPPD_ARATH	HPD	0.83
	Val, Ile, Leu	2-oxoisovalerate dehydrogenase subunit alpha 2, mitochondrial	ODBA2_ARATH		1.18
		2-oxoisovalerate dehydrogenase subunit beta 1, mitochondrial	ODBB1_ARATH	BCDH BETA1	0.64

(continued)

© 2019 The Authors

Table 1. (continued)

Biological process	Subcategory	Compound[a]	blastP	Gene name	log_2 ratio
		Methylcrotonyl-CoA carboxylase subunit alpha, mitochondrial	MCCA_ORYSJ	MCCA	0.77
		Methylcrotonyl-CoA carboxylase beta chain, mitochondrial	MCCB_ARATH	MCCB	0.82
Lipid catabolism	Fatty acids	Glyoxysomal fatty acid beta-oxidation multifunctional protein MFP-a	MFPA_CUCSA		1.02
		Malate dehydrogenase, glyoxysomal	MDHG_CITLA		−2.26
		Acyl-coenzyme A oxidase 3, peroxisomal	ACOX3_ARATH	ACX3	1.13
		Long chain acyl-CoA synthetase 7, peroxisomal	LACS7_ARATH	LACS7	0.68
		3-ketoacyl-CoA thiolase 2, peroxisomal	THIK2_ARATH	PED1	0.68
	Galactolipids	Phospholipase A1-Ibeta2, chloroplastic	PLA14_ARATH		1.25
		Patatin-like protein 2	PLP2_ARATH	PLP2	3.79
	Mono-diacylglycerol	Monoacylglycerol lipase	MGLL_MYCTU		0.9
	Tri-acylglycerol	Lipase	LIP_RHIMI		0.71
		Lipase	LIP_RHIMI		2.57
		Triacylglycerol lipase SDP1	SDP1_ARATH	SDP1	1.57
Lipid biosynthesis	Cuticle	Protein ECERIFERUM 26	CER26_ARATH	CER26	−1.86
		3-ketoacyl-CoA synthase 6	KCS6_ARATH	CUT1	−0.83
		3-ketoacyl-CoA synthase 10	KCS10_ARATH	FDH	−1.2
		Glycerol-3-phosphate 2-O-acyltransferase 6	GPAT6_ARATH	GPAT6	−1.31
	Fatty acids	Stearoyl-[acyl-carrier-protein] 9-desaturase, chloroplastic	STAD_ELAGV		−0.61
		Biotin carboxyl carrier protein of acetyl-CoA carboxylase	BCCP_NOSS1	accB	−0.66
		Acetyl-CoA carboxylase carboxyl transferase subunit beta	ACCD	accD	−1.02
		Omega-3 fatty acid desaturase, chloroplastic	FAD3C_SESIN	FAD7	−0.96
		3-oxoacyl-[acyl-carrier-protein] synthase II, chloroplastic	KASC2_ARATH	KAS2	−1
		Palmitoyl-[acyl-carrier-protein] 4-desaturase 3, chloroplastic	STAD3_OPHSP	SAD3	−0.63
	Galactolipids	Digalactosyldiacylglycerol synthase 1, chloroplastic	DGDG1_SOYBN	DGD1	−0.53
		Probable monogalactosyldiacylglycerol synthase, chloroplastic	MGDG_SOYBN	MGD A	−1.06
Glyoxylate cycle		Malate synthase, glyoxysomal	MASY_CUCSA		1.5
		Isocitrate lyase (EP)	ACEA_DENCR	ICL	3.79
Gluco-neogenesis		Fructose-1,6-bisphosphatase, cytosolic	F16P2_ORYCO		−1.89
		Phosphoenolpyruvate carboxykinase	PCKA_ARATH	PCKA	0.76
		Pyruvate, phosphate dikinase, chloroplastic	PPDK_MESCR	PPD	−1.52
Oxidative stress	Ascorbate glutathione cycle	Probable L-ascorbate peroxidase 4, peroxisomal	APX4_ORYSJ	APX4	−0.88
		Putative L-ascorbate peroxidase 6	APX6_ARATH	APX6	−0.61
		Glutathione reductase, chloroplastic	GSHRP_TOBAC	GOR	−0.67
		Putative glutathione peroxidase 7, chloroplastic	GPX7_ARATH	GPX7	−1.04
	Antioxidant enzymes	Superoxide dismutase [Fe] 2, chloroplastic	SODF2_ORYSJ		−0.63
		OXIDATIVE STRESS 3 (OXS3)?	NA	OXS3	2.33
		Peroxidase 73	PER73_ARATH	PER73	2.37
		Peroxiredoxin-2C	PRX2C_ORYSJ	PRXIIC	−0.96
		Peroxiredoxin-2E, chloroplastic	PRX2E_ARATH	PRXIIE	−0.97
		Peroxiredoxin Q, chloroplastic	PRXQ_POPJC	PRXQ	−1.52
Biotic stress		Chitinase 2	CHIT2_TULBA		1.07
		Nematode resistance protein-like HSPRO2	HSPR2_ARATH	HSPRO2	2.13
		Protein HYPER-SENSITIVITY-RELATED 4	HSR4_ARATH	HSR4	2.37
		Polygalacturonase inhibitor 1	PGIP1_ARATH	PGIP1	1.74
		Putative disease resistance protein RGA4	RGA4_SOLBU	RGA4	0.93
		Probable WRKY transcription factor 23	WRK23_ARATH	WRKY23	1
		Probable WRKY transcription factor 28	WRK28_ARATH	WRKY28	2.15

(continued)

© 2019 The Authors
The Plant Journal © 2019 John Wiley & Sons Ltd,

Table 1. (continued)

Biological process	Subcategory	Compound[a]	blastP	Gene name	log_2 ratio
		Probable WRKY transcription factor 35	WRK35_ARATH	WRKY35	2.08
		Probable WRKY transcription factor 40	WRK40_ARATH	WRKY40	1.6
		Probable WRKY transcription factor 48	WRK48_ARATH	WRKY48	1.01
		Probable WRKY transcription factor 50	WRK50_ARATH	WRKY50	1.64
		Probable WRKY transcription factor 70	WRK70_ARATH	WRKY70	1.14
		Probable WRKY transcription factor 75	WRK75_ARATH	WRKY75	2.34
Senescence		Apoptosis-inducing factor homolog A	AIFA_DICDI	aifA	1.5
		Apoptosis-inducing factor homolog A	AIFA_DICDI	aifA	1.58
		Autophagy-related protein 11	ATG11_ARATH	ATG11	0.65
		Autophagy-related protein 13a	AT13A_ARATH	ATG13A	0.83
		Autophagy-related protein 18a	AT18A_ARATH	ATG18A	0.82
		Autophagy-related protein 2	ATG2_ARATH	ATG2	0.8
		NAC transcription factor 29	NAC29_ARATH	NAC029	2.78
		Programmed cell death protein 4	PDCD4_CHICK	PDCD4	1.68
		WRKY transcription factor 6	WRKY6_ARATH	WRKY6	1.41
Senescence inhibition		BES1/BZR1 homolog protein 4	BEH4_ARATH	BEH4	−0.56
Nucleic acids degradation		Endonuclease 2	ENDO2_ARATH	ENDO2	3.12
Protein degradation	Proteasome	E3 ubiquitin-protein ligase ATL6	ATL6_ARATH	ATL6	0.89
		E3 ubiquitin-protein ligase ATL6	ATL6_ARATH	ATL6	1.23
		BTB/POZ and TAZ domain-containing protein 1	BT1_ARATH	BT1	3.03
		Proteasome activator subunit 4	PSME4_ARATH	PA200	1.11
		F-box protein PP2-A13	P2A13_ARATH	PP2A13	0.89
		F-box protein SKP2A	SKP2A_ARATH	SKP2A	1
	Protease	Cysteine proteinase 2	CYSP2_MAIZE	CCP2	−0.77
		Protease Do-like 1, chloroplastic	DEGP1_ARATH	DEGP1	−0.72
		Protease Do-like 8, chloroplastic	DEGP8_ARATH	DEGP8	−1.05
		ATP-dependent zinc metalloprotease FTSH 11, chloroplastic/mitochondrial	FTSHB_ARATH	FTSH11	−0.86
		ATP-dependent zinc metalloprotease FTSH 2, chloroplastic	FTSH2_ARATH	FTSH2	−0.87
		Subtilisin-like protease SBT1.4	SBT14_ARATH	SBT1.4	−1.03
		Subtilisin-like protease SBT1.7	SBT17_ARATH	SBT1.7	−1.23
		Subtilisin-like protease SBT2.6	SBT26_ARATH	SBT2.6	−1.66
		Subtilisin-like protease SBT3.17	SBT3H_ARATH	SBT3.17	−0.92
		Serine carboxypeptidase-like 27	SCP27_ARATH	SCPL27	−1.13
		Serine carboxypeptidase-like 34 (CD)	SCP34_ARATH	SCPL34	−1.62
		Serine carboxypeptidase-like 45	SCP45_ARATH	SCPL45	−0.82

[a]Species displaying a statistically different result are indicated in brackets (CD: *C. damasonium*, EH: *E. helleborine*, EP: *E. purpurata*). See Data S1 for pair-specific responses.
[b]This plastidial isoform of BCAA aminotransferase is normally involved in biosynthetic processes, however we failed to detect isoforms involved in the catabolic pathway, raising the possibility that reads from catabolic isoforms have been wrongly associated with biosynthetic isoforms.

was 10× less abundant (Table S1). These differences correlated with a higher N content in albinos compared with their green counterparts (4.1 ± 0.66% mean dry weight ± 95% confidence interval versus 3.2 ± 0.38%, $P = 0.019$, $t = 3.03$, d.f. = 7, paired two-sided Student's *t*-test; Figure S2).

Asparagine synthetase (*ASNS_ASPOF*) and asparaginase (*ASPGB_ARATH*) showed a strong induction (11×) and repression (8×), respectively, in line with high asparagine levels in albinos (Table 1). Shikimate abundance was lower in albinos, pointing to a possible inhibition of the shikimate pathway and the associated aromatic amino acid biosynthesis (Figure 1; Table S1). The expression of most other amino acid biosynthesis enzymes was not altered, except for cysteine (repression of *APR3* and *RCS3*) and branched-chain amino acids (BCAA: valine, isoleucine, leucine), which showed contrasting results with some evidence of repression (*IPMSA*, *IIL1*) and uncertain induction (*BCAT3*; Table 1, see footnote a).

© 2019 The Authors

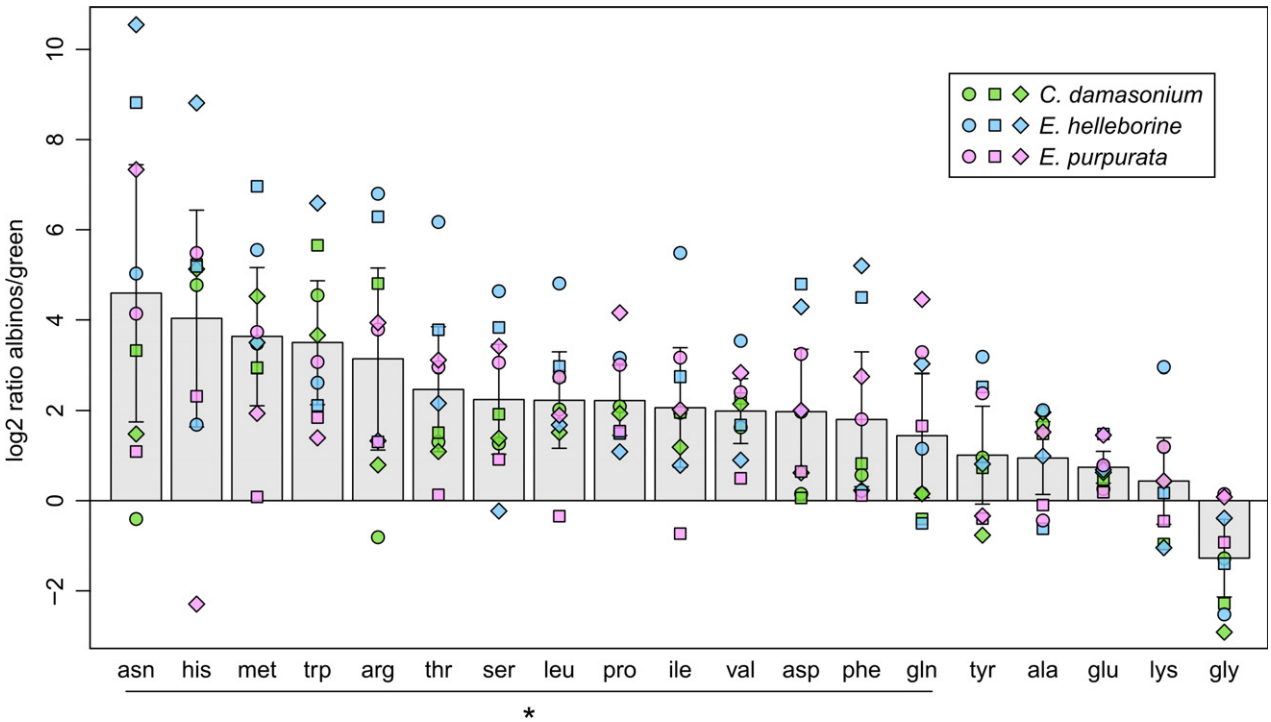

Figure 3. Changes in amino acids levels in albino leaves compared with green ones. Each point represents the log2 ratio of one albino/green pair. Mean values ± 95% confidence intervals for the nine replicates are shown. Colours indicate species and symbols populations. The bar with a star shows amino acids that are significantly more abundant in albino leaves (see Table S1). Cysteine was not detected by GC-MS.

Higher hexoses, amino acids and fatty acid degradation for energy production

Sucrose and fructose were far less abundant in albinos (respectively 6× and 10×; Figure 1; Table S1), and, indeed, sucrose-phosphate synthase was repressed (*SPS*; Table 1), consistently with the absence of photosynthesis. Some other secondary carbohydrates showed a similar response (mannose, xylose, arabinose), whereas many did not change (glucose, ribose, rhamnose, xylulose, trehalose, maltose, lactose), including glucose-6P and fructose-6P (Figure 1; Table S1). Sucrose degradation enzymes were induced (*IVR1*, *CIN3*, *NIN1*) as well as transporters of sucrose and other sugars (*SUT1*, but *SUT2* was repressed, *SWEET2A*, *STP13*, *ERDL6_ARATH*; Table 1). Trehalase was highly induced in albinos (*TRE_ORYSJ*), suggesting an increase in trehalose degradation (Table 1). As for trehalose-6P, both synthesis and degradation enzymes were induced in albinos (*TPS5*, *TPS6*, *TPS9*, *TPP2*, but *TPP6* was repressed; Table 1), pointing to a possible role for this intermediate in albino metabolism.

Cytosolic glycolysis, oxidative pentose phosphate pathway (OPPP) and tricarboxylic acid cycle (TCA) were not evidently altered from gene expression or metabolic intermediate abundance, whereas many plastidial isoforms of glycolytic and OPPP enzymes were repressed (Table S1).

Several genes involved in amino acid catabolism were induced in albino (Table 1), such as those involved in the degradation of glutamate (*GDH1*), proline (*POX2*), arginine (*OAT*), lysine (*LKR/SDH*), BCAA (*ODBA2_ARATH*, *ODBB1_ARATH*, *MCCA*, *MCCB*, *PED1*, *ACX3*) and tyrosine (*HPD*, *HGO*). In addition to, some amino acid transporters were also induced in albinos (*BAT1*, *AAP7*, *AATL1*, *PROT2_ORYSJ*), suggesting a high reliance on import and subsequent degradation of amino acids for energy production (Table 1).

Several lipases were induced, suggesting a higher production of fatty acids from galactolipids (*PLP2*, *PLA14_ARATH*), triacylglycerols (*SDP1*, *LIP_RHIMI*), monoacylglycerols and diacylglycerols (*MGLL_MYCTU*; Table 1). The main enzymes for fatty acid degradation were also expressed at higher levels in albinos (*LACS7*, *ACX3*, *MFPA_CUCSA*, *PED1*; Table 1). Curiously, peroxisomal malate dehydrogenase (*MDHG_CITLA*), which ensures NAD^+ regeneration for β-oxidation, was strongly repressed in albinos (Table 1). Moreover, enzymes involved in fatty acid biosynthesis, which occur in part in plastids, were generally repressed in albinos (*ACCB*, *ACCD*, *KAS2*, *SAD3*, *STAD_ELAGV*, *FAD7*) as well as those synthesizing galactolipids (*MGDA*, *DGD1*) and cuticle compounds (*GPAT6*, *CUT1*, *FDH*, *CER26*; Table 1).

Activation of the glyoxylate cycle in albinos

Peroxisomal isocitrate lyase (*ICL*) and malate synthase (*MASY_CUCSA*), two key enzymes of the glyoxylate cycle, were highly induced in *C. damasonium* and *E. helleborine*

© 2019 The Authors
The Plant Journal © 2019 John Wiley & Sons Ltd,

albinos, while this was less clear for *E. purpurata* (Table 1). The glyoxylate cycle produces succinate from acetyl-CoA (e.g. issuing from lipid catabolism), which, after conversion to oxaloacetate in mitochondria, can enter gluconeogenesis in the cytosol. Although the phospho-enol-pyruvate carboxykinase (*PCKA*) expression was slightly induced, the other gluconeogenesis enzyme pyruvate orthophosphate dikinase (*PPD*) and fructose-1,6-bisphosphatase (*F16P2_ORYCO*) were markedly repressed, making it uncertain that organic acids produced by the glyoxylate cycle were further processed into sugars.

Different responses to stress in albinos and possible autophagy induction

Lower dehydroascorbate level, lower expression of ascorbate glutathione cycle enzymes (*GOR*, *APX4*, *APX6*, *GPX7*) and other antioxidant enzymes (*PRXIIC*, *PRXIIE*, *PRXQ*, *SODF2_ORYSJ*) indicated reduced level of oxidative stress in albinos, although few antioxidant genes were induced (*PER73*, *OXS3*; Table 1).

No clear evidence of alteration in other abiotic stress responses (especially drought) was observed in albinos (Data S1). However, many genes induced during defence against pathogens were more expressed (*CHIT2_TULBA*, *PGIP1*, *HSR4*, *HSPRO2*, several *WRKY* transcription factors), suggesting a higher level of pest attacks against albinos (Table 1).

Some autophagy and senescence-related genes were also induced in albinos (*ATG2*, *ATG11*, *ATG13A*, *ATG18A*, *NAC029*, *WRKY6*, *PDCD4*, *AIFA*), as well as one endonuclease (*ENDO2*) and some proteasome-related genes (*PA200*, *PP2A13*, *BT1*, *SKP2A*, *ATL6*; Table 1). Although other peptidases potentially active during autophagy were repressed (*CCP2*, several members of the *SBT*, *DEGP*, *FTSH* and *SCPL* families), increase in proteolysis level characterizing albinos.

DISCUSSION

The occurrence and growth of albinos *in natura* within green mixotrophic orchids suggests a specific metabolism in these species, compared with normal autotrophic plants. To identify potential specific features of mixotrophic orchids, we studied the physiology of spontaneous albinos through their transcriptome and metabolome, across three species and eight populations. We observed numerous conserved responses to albinism across these species. Here, we compared our results with other cases of photosynthesis loss in plants to provide clues about potential specific features of mixotrophic orchids.

Albinos' response to photosynthesis loss is similar to that of white parts of variegated leaves

Our results are particularly reminiscent of studies on variegated plants. Variegation is another model of natural, non-lethal achlorophylly in which leaves exhibit achlorophyllous sectors interspersed with green, photosynthetic ones. Variegation also occurs in plants with a juxtaposition of white and green leaves or twigs. Achlorophyllous sectors in variegated plants survive thanks to surrounding functional photosynthetic areas, and allow comparison with mixotrophic albinos that survive on fungal resources. Transcriptomic and metabolomic studies of variegated *Arabidopsis thaliana* (Aluru *et al.*, 2009; Figure S3) and *Pelargonium x hortorum* (Tcherkez *et al.*, 2012; Abadie *et al.*, 2016) revealed trends remarkably similar to our observations. Achlorophyllous sectors show lower sugar level, higher uptake and degradation of sucrose, no evident alteration of glycolysis and TCA cycle, lower nitrogen assimilation, strong induction of asparagine synthetase, higher levels of free amino acids, higher (respectively lower) catabolism (respectively biosynthesis) of amino acids and fatty acids, induction of the glyoxylate cycle enzyme isocitrate lyase (Aluru *et al.*, 2009; Tcherkez *et al.*, 2012; Abadie *et al.*, 2016). Variegated plants also showed higher expression of genes involved in biotic stress: in albinos, higher herbivore pressure, expected from nitrogen enrichment and more conspicuous colour, has indeed been documented together with higher fungal infection in the albino *C. damasonium* (Roy *et al.*, 2013).

A response to carbon starvation characterizes albino metabolism

Other metabolic changes were strikingly parallel to those during the carbon starvation response, in a way also conserved in variegated plants (Figure 4). Some metabolic changes closely resembled features of carbon-starving cells: increase in sugars and amino acid transporters (Contento *et al.*, 2004; Buchanan-Wollaston *et al.*, 2005), increase in sucrose-degrading enzymes (Buchanan-Wollaston *et al.*, 2005; Baena-González *et al.*, 2007), alteration of trehalose metabolism (Baena-González *et al.*, 2007; Lunn *et al.*, 2014; Garapati *et al.*, 2015), increase in free amino acids (Brouquisse *et al.*, 1998; Araújo *et al.*, 2010; Hirota *et al.*, 2018), induction of asparagine synthetase (Brouquisse *et al.*, 1992; Baena-González *et al.*, 2007), higher catabolism of amino acids (Contento *et al.*, 2004; Baena-González *et al.*, 2007; Araújo *et al.*, 2010; Garapati *et al.*, 2015; Hirota *et al.*, 2018), induction of lipases (Buchanan-Wollaston *et al.*, 2005; Baena-González *et al.*, 2007), fatty acid β-oxidation enzymes (Pistelli *et al.*, 1992; Baena-González *et al.*, 2007), glyoxylate cycle enzymes (Pistelli *et al.*, 1992; Chen *et al.*, 2000; but not in Charlton *et al.*, 2005), and higher expression (respectively repression) of autophagy-promoting (respectively inhibiting) genes (Garapati *et al.*, 2015; Üstün *et al.*, 2017; Hirota *et al.*, 2018). Carbon-starved cells actively degrade their components, especially by enclosing them in autophagosomes addressed to the vacuole, where proteolysis

© 2019 The Authors

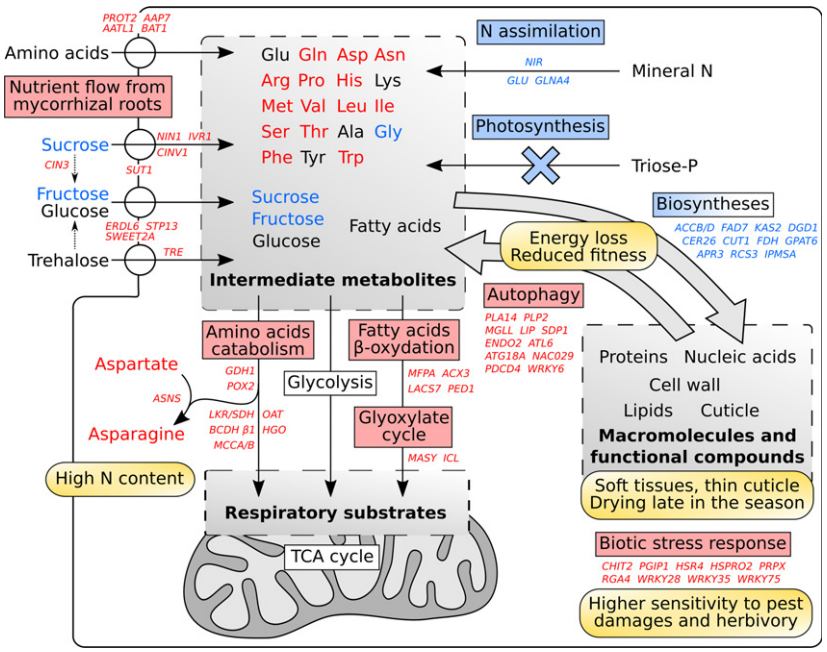

Figure 4. Summary of the metabolic changes triggered by albinism. Red (respectively blue) indicates higher (respectively lower) metabolite abundance or gene expression (Tables S1 and 1). Boxes indicate major molecular pathways that are induced (red), repressed (blue) or unaltered (white). Most of these changes are symptomatic of the carbon starvation response. Yellow rounded boxes draw links with phenotypic observations.

releases amino acids as nutrients (Brouquisse *et al.*, 1998; Diaz-Mendoza *et al.*, 2016; Hirota *et al.*, 2018). Although we detected no specific protease induction, an activation of autophagy-driven proteolysis in albinos would fit with the transcriptomic observations mentioned above as a consequence of the carbon starvation response.

The reduction in available sugars (especially sucrose and fructose) in albinos is likely to trigger cellular starvation, as would happen in a photosynthetic cell placed in the dark. Autophagy enables cell survival for up to several days, by releasing nutrients for energy production (Üstün *et al.*, 2017), but if adverse conditions persist, carbon starvation ultimately leads to cell death. Albinos still receive enough nutrients from fungi to survive as long as purely autotrophic plants (Shefferson *et al.*, 2016), and the sampled albinos displayed normal growth, without visible senescence. Yet, later in the growth season, many albino leaves and even some full shoots undergo a 'drying' process (Roy *et al.*, 2013) starting as local necrosis (see Appendix B in Roy *et al.*, 2013), which may arise from excessive autophagy.

Autophagy uses resources provided by the fungus that supported the early shoot growth in the spring (Roy *et al.*, 2013; Gonneau *et al.*, 2014), and it therefore should be viewed as a delayed, indirect use of fungal resources. Continuous autophagy implies costly recycling of cellular components, and presumably harms or destroys structures vital for other cellular functions. This may enhance cell dysfunctions, especially late in the growth season where fungal colonization is at its lowest (Roy *et al.*, 2013; Gonneau *et al.*, 2014). Several observations of albinos support carbon limitation, because they sometimes display: (i) lower size and flower number than green individuals (Salmia, 1989; Roy *et al.*, 2013; Shefferson *et al.*, 2016; but see Julou *et al.*, 2005); (ii) less frequent shoot survival until seed production (Roy *et al.*, 2013; Gonneau *et al.*, 2014); (iii) reduced level of carbon-rich support tissues (Salmia, 1989) and a thinner cuticle (by ca. 2×; Roy *et al.*, 2013 – a trend congruent with our observations of lower expression of genes involved in biosynthesis of cuticle compounds); (iv) higher specific leaf area (4× lower leaf thickness; Roy *et al.*, 2013), which may result from cell wall biosynthesis limitation and/or autolytic processes; and (v) a 3-4× reduction in basal metabolism (as estimated from respiration in the dark; Julou *et al.*, 2005; Roy *et al.*, 2013).

Evolved as a way to cope with constraints on carbon supply, the starvation response ironically seems to act as a genetic burden in albinos, reducing their fitness. It furthermore hides any possible more subtle metabolic changes specific to mycoheterotrophy and makes challenging determination of what is primarily used by albino cells.

Imported sugars and amino acids are probably major resources for albino leaves

Sugars, the main form of carbon transport in plants, are likely to fulfil large parts of albino carbon needs. Among these, sucrose is preferentially used in most plants, including orchids (Ng and Hew, 1996), and is therefore expected to be transferred to albino sink tissues from mycorrhizal roots receiving fungal carbon. Whereas sucrose and fructose decreased in albino cells as a consequence of photosynthesis loss, glucose levels remained unchanged, suggesting a specific compensatory flux independent of sucrose intake. In the absence of detected gluconeogenesis

© 2019 The Authors
The Plant Journal © 2019 John Wiley & Sons Ltd,

or any other glucose-producing pathway, glucose is likely to have had an exogenous source. It could be transferred as such, or through complex sugars such as trehalose, whose level is not altered as compared with green individuals. However, the carbon starvation response blurs interpretations as it significantly alters trehalose metabolism: indeed, trehalose-6P (T6P) is a sensor of the cell's carbon status that mediates the starvation response and coordinates plant growth (Lunn *et al.*, 2014; Garapati *et al.*, 2015). Induction of both T6P synthesis and degradation enzymes (*TPS* and *TPP*) on the one hand, and trehalase on the other hand, may affect trehalose level by enabling interconversion of glucose and trehalose. It is therefore, uncertain whether the inflow of carbohydrates into the leaf cells involves glucose or trehalose. Trehalose has nevertheless already been suggested as a form of sugar transported from fungi to orchids (Smith and Read, 2008) that can be assimilated in orchid leaves (Smith and Smith, 1973). Experimental testing (e.g. by fungal labelling) of long-distance sugar transport is needed to define the role of sugars in albinos better.

Albinos are dependent on external organic nitrogen, as supported by induction of amino acid transporters and repression of nitrogen assimilation. Fochi *et al.* (2017) recently showed that at the stage of mycoheterotrophic germination in the rhizoctonia-associated orchid *Serapias vomeracea*, organic nitrogen is transferred from rhizoctonias to the plant. N-rich amino acids such as arginine, lysine and histidine are probably exported from living fungal cells (Fochi *et al.*, 2017). Although our albino orchids associate mainly with non-rhizoctonia ectomycorrhizal fungi (e.g., Julou *et al.*, 2005), a similar flow of organic nitrogen may occur so that leaves receive amino acids, either from fungi or following their processing in roots, as already suggested by Suetsugu *et al.* (2017). In addition to being a nitrogen source, amino acids also represent an energy source for albinos facing carbon limitation, as their carbon skeleton yields respiratory substrates (Araújo *et al.*, 2011), while excessive nitrogen is diverted to N-rich storage molecules such as asparagine (Zrenner *et al.*, 2006; Hildebrandt *et al.*, 2015). Among amino acids, lysine and BCAA degradation allows a particularly high energy yield by directly providing electrons to the mitochondrial electron transport chain during the oxidation of their derivatives isovaleryl-CoA and hydroxyglutarate (Araújo *et al.*, 2011; Hildebrandt *et al.*, 2015). Interestingly, lysine levels did not follow the general increase observed for other amino acids in albinos. Together with strong induction of the enzyme catalyzing the first step of lysine degradation, this supports major use of lysine as an energy source. A similar reasoning applies to BCAA, which is moderately accumulated in albinos as compared with other amino acids and whose degradation enzymes seem induced. We note that expression of the enzymes supplying electrons to the mitochondrial electron transport chain during lysine and BCAA catabolism showed no variation in albinos (*IVD_ORYSJ*, *D2HGDH*, *ETFA*, *ETFB*, *ETFQO_ORYSJ*, Data S1), but this step may not be limiting in energy production from these amino acids.

Interestingly, in addition to sucrose, white sectors of variegated *P.* × *hortorum* also receive amino acids from photosynthetic sectors (Tcherkez *et al.*, 2012; Abadie *et al.*, 2016). This stresses the need for dedicated labelling experiments to clarify the nature of the transferred nitrogenous compounds in mixotrophic orchids. Amino acid uptake and catabolism, which is already important at mycoheterotrophic orchid germination (Fochi *et al.*, 2017), may partly circumvent carbon limitation, and their use at adulthood may be crucial in the evolution of mycoheterotrophic orchids.

Evolutionary perspectives

Although usually lethal at whole organism level, albinism in mixotrophic orchids did not dramatically alter development. Here, we showed that this ability does not seem to be associated with any major alteration of the metabolism of these orchids: indeed, the global change in transcriptome between albinos and green individuals was within the natural variability of gene expression for each phenotype among different sites (Figure S1). The induction of the carbon starvation response, a legacy from photosynthetic progenitors, explains most identified transcriptome and metabolome changes in response to albinism. Although we have certainly missed information for unknown genes, we observed no specific changes related to the ability to sustain albinism in these three mixotrophic orchid species. This parallels the investigations of Suetsugu *et al.* (2017) in which very limited transcriptomic changes were observed between mycorrhizal roots of albino and green *E. helleborine* individuals. Therefore, rather than major metabolic novelty, functional response to albinism relies on existing pathways and a suitable carbon source, namely the exploitation of fungi that deliver sugars and amino acids, the latter especially helping to alleviate carbon starvation (Figure 4).

The absence of a major metabolic response to albinism specific to these orchids has to be considered in the framework of the mixotrophic status of these species, which inherently rely on fungal nutrients for rhizome resources (Gonneau *et al.*, 2014; Lallemand *et al.*, 2019) and during early shoot development at least (Roy *et al.*, 2013; Gonneau *et al.*, 2014; Těšitel *et al.*, 2018). Indeed, green individuals in mixotrophic species already handle the restriction of photosynthesis during their vegetative growth, due to environmental conditions (Julou *et al.*, 2005) or limited intrinsic photosynthetic abilities (Girlanda *et al.*, 2006). However, fruits and seeds are more dependent on photosynthetates, especially from capsules and leaves (Bellino

© 2019 The Authors

et al., 2014; Gonneau *et al.*, 2014; Suetsugu *et al.*, 2018; Těšitel *et al.*, 2018; Lallemand *et al.*, 2019), and make limited use of fungal nutrients, either for physiological reasons or because fungal mycorrhizal colonization reaches a minimum at fruiting time (Roy *et al.*, 2013; Gonneau *et al.*, 2014).

Our results support an exaptation in which nitrogen nutrition is used to get fungal carbon in mixotrophic orchids, in a way reminiscent of what happens at germination in rhizoctonia-associated autotrophic orchids (Fochi *et al.*, 2017), as suggested in the 'carbon hitchhiking' hypothesis of Selosse and Roy (2009). In this respect, mixotrophy would be a pedomorphosis, i.e. an evolutionary novelty extending to adulthood traits present at the juvenile stage in the ancestors and extent relatives. The shift in fungal partners in mixotrophs, from rhizoctonia partners to ectomycorrhizal fungi, may not reflect a different plant–fungal exchange, but simply resulted from other constraints such as a higher flow of resources (Merckx *et al.*, 2013b; Selosse and Martos, 2014; Jacquemyn *et al.*, 2017).

Albinos fitness may be limited by the cost of a permanent starvation response and of the related autophagy. Any mutation impairing starvation stress sensing or autolytic processes would therefore improve albinos fitness and favour speciation by way of albinism, as proposed earlier (Shefferson *et al.*, 2016). Comparative genomic studies among Neottieae species would surely clarify the molecular bases of this evolution, as this lineage exhibits repeated independent shifts to mycoheterotrophy (Selosse and Roy, 2009; Feng *et al.*, 2016). Parasitic plants such as *Striga* or *Cuscuta* (Press *et al.*, 1991) are other mixotrophic lineages in which photosynthesis can be partially or completely lost and carbon is acquired from their host (Těšitel *et al.*, 2018). Replicating investigations on metabolic pathways involved in the nutrition of these other lineages are crucial in future research to understand the loss of photosynthesis in plant evolution.

EXPERIMENTAL PROCEDURES

Species analyzed and sampling procedure

Cephalanthera and *Epipactis* populations from France and Luxembourg for which albinos have been reported were visited during the spring and summer of 2016. For each site, we selected one (two for the population at Boigneville) albino and one (two at Boigneville) green counterpart growing nearby with similar size, phenology and light condition (Figure 5). Light condition was measured as photosynthetically active radiation (PAR) and expressed as photosynthetic photon flux density (PPFD) summed from 400 to 700 nm with a MQ-200 Quantum Meter (Apogee Instruments). For each selected individual, one leaf was cut and immediately frozen in liquid nitrogen. Care was taken to sample leaves with no senescence or pathogen damage mark, and to choose leaves of similar developmental stage for each albino/green pair. We ended up with a final set of three species with three biological replicates for each (Table 2).

Figure 5. An albino/green pair: *Epipactis helleborine* at Poncin (France). The albino stalk chosen for analysis is the one at the forefront. Picture by F. Lallemand.

N content measurements

N contents of albino and green leaves were estimated using a continuous flow elemental analyzer (EA Thermo Flash 2000). Samples were ground and around 1 mg of leaf powder was analyzed. Alanine was used as an internal standard. Mean values ± standard deviation for alanine N content were 15.82% ± 0.21 and 15.70% ± 0.39 (two runs, $n = 15$ for each) compared with an expected theoretical value of 15.72%. Data were consequently corrected.

Metabolomic gas chromatography – mass spectrometry (GC-MS) analyses

The ground frozen samples (60–66 mg fresh weight) was resuspended in 1 mL of frozen (−20°C) water: acetonitrile: isopropanol (2:3:3) containing 4 pg mL^{-1} ribitol and extracted for 10 min at 4°C with shaking at 1500 rpm in an Eppendorf thermomixer. Insoluble material was removed by centrifugation at 19500 ***g*** for 10 min. 100 μL was collected and 10 μL of 30 pg mL^{-1} myristic acid d27 were added as an internal standard for retention time locking. Extracts were dried for 4 h at 35°C in a Speed-Vac evaporator and stored at −80°C.

All steps of GC-MS analyses were done as in Fiehn (2006) and Fiehn *et al.* (2008). Samples were taken out of −80°C, warmed for 15 min before opening and Speed-Vac evaporator dried again for 1.5 h at 35°C before adding 10 μL of 20 mg mL^{-1} methoxylamine in pyridine to the samples and the reaction was performed for 90 min at 30°C with continuous shaking in an Eppendorf thermomixer. 90 μL of *N*-methyl-*N*-trimethylsilyl-trifluoroacetamide (MSTFA) (Regis Technologies 1-270590-200; 10× 1 g) was then added and the reaction continued for 30 min at 37°C. After cooling, 100 μl was transferred to an Agilent vial for injection.

Four hours after derivatization, 1 μl of sample was injected in a splitless mode on an Agilent 7890B gas chromatograph coupled to an Agilent 5977A mass spectrometer. The column was a Rxi-5SilMS from Restek (30 m with 10 m Integra-Guard column – ref 13623-127). An injection in split mode with a ratio of 1:30 was systematically performed for saturated compound quantification. The oven temperature ramp was 60°C for 1 min then 10°C/min to 325°C for 10 min. Helium constant flow was 1.1 mL min^{-1}. Temperatures were the following: injector: 250°C, transfer line: 290°C,

© 2019 The Authors
The Plant Journal © 2019 John Wiley & Sons Ltd,

Table 2 Summary of the species and populations sampled. All the sites are located in France except Kayl (Luxembourg)

Species	Site	Code	Sampling date	Sampling time	Localisation (decimal degrees WGS 84)	PAR (PPFD, μmol m^{-2} sec^{-1})	Phenology
Cephalanthera damasonium	Mesnil-Soleil	CD1	25/05/16	11:00	48.9258°N, 0.1375°W	18	Flowering
	Boigneville[a] (two pairs)	CD2	06/06/16	12:20	48.3399°N, 2.3600°E	25	Flowering
		CD3					Flowering
Epipactis helleborine	Poncin	EH1	19/05/16	11:20	46.1074°N, 5.4519°E	245	Leaves development
	Villeneuve	EH2	30/05/16	10:40	43.3356 N, 2.4806°E	1220	Flower buds
	Kayl	EH3	22/07/16	11:00	49.4791 N, 6.0212°E	87	Flower buds
Epipactis purpurata	Hirtzbach	EP1	19/07/16	11:30	47.5856 N, 7.2139°E	136	Flower buds
	Evosges	EP2	21/07/16	15:20	45.9486 N, 5.5113°E	8	Flower buds
	Levier	EP3	04/08/16	15:00	46.9405 N, 6.0767°E	2	Flower buds

[a]This population has already been investigated for photosynthetic rates and mycorrhizal partners of albinos (Julou *et al.*, 2005), genetic diversity (Tranchida-Lombardo *et al.*, 2010), fitness (Roy *et al.*, 2013) and survival (Shefferson *et al.*, 2016).

source: 230°C and quadrupole 150°C. The quadrupole mass spectrometer was switched on after a 5.90 min solvent delay time, scanning from 50 to 600 u. Absolute retention times were locked to the internal standard d27-myristic acid using the Retention Time Locked (RTL) system provided in Agilent's Masshunter software. Retention time locking reduces run-to-run retention time variation. Samples were randomized. A fatty acid methyl ester mix (C8, C9, C10, C12, C14, C16, C18, C20, C22, C24, C26, C28, C30) was injected in the middle of the queue for external Retention Index calibration.

Raw Agilent data files were analyzed with AMDIS (http://chemdata.nist.gov/mass-spc/amdis/). The Agilent Fiehn GC/MS Metabolomics RTL Library (version June 2008) was employed for metabolite identifications. Peak areas were determined with the Masshunter Quantitative Analysis (Agilent) in splitless and split 30 modes. Because automated peak integration was occasionally erroneous, integration was verified manually for each compound in all analyzes. Resulting areas were compiled in one single Excel File for comparison. Peak areas were normalized to ribitol and fresh weight. Metabolite contents are expressed in arbitrary units (semi-quantitative determination).

RNA extraction

In total, 100 mg of fresh material per sample was extracted using the NucleoZOL protocol (Macherey-Nagel, France). A DNase treatment (DNase Max, Qiagen, France) was then performed followed by a final purification with the Agencourt RNAclean xp kit (Beckman, France). The integrity of total RNAs was checked on an RNA Nanochip using Agilent 2100 bioanalyzer (Agilent Technologies, Waldbroon, Germany).

Sequencing and quality trimming

The RNA-seq experiment was carried out at the Institute of Plant Sciences Paris-Saclay (IPS2, Saclay, France). The libraries were constructed using the TruSeq Stranded Total RNA with Ribo-Zero Plant Leaf kit (Illumina®, California, USA) following the supplier's instructions. They were then sequenced in multiplex with a NextSeq500 high output v2 kit in paired-end (PE) with a read length of 150 bases. After quality trimming with Trimmomatic (v0.36, parameters TruSeq3-PE.fa:2:30:10:2:true MINLEN:30; Bolger *et al.*, 2014), between 21 684 667 and 27 138 011 (average 23.2 million) pairs of read per sample were generated.

De novo transcriptome assembly and annotation

The *de novo* assembly of the transcriptome was performed following Roberts and Roalson (2017). Briefly, for each species, 16 assemblies were generated. One with Trinity (v2.3.2, default parameters except –SS_lib_type RF –min_kmer_cov 3; Haas *et al.*, 2013) on all the samples and 15 with Velvet-Oases (v1.2.09; Schulz *et al.*, 2012) corresponding to five assemblies (with kmers 25, 35, 45, 55 and 65) for each of the three sites. The assembly with Velvet-Oases on the pool of all the samples failed regardless of the parameters. These 16 assemblies were then combined with the tr2aacds.pl script (v2014.05.15) of the EvidentialGenes suite (Nakasugi *et al.*, 2014). Only contigs classified as 'main' were kept in the final unigene set. The quality of the unigene set for each species was assessed with BUSCO v3.0.2 (Waterhouse *et al.*, 2018) using hmmer 3.1b2 against the embryophyta_odb9 dataset. The contigs were annotated with the Blast and Pfam analyzes of Trinotate v3. The uniprot_sprot.pep and Pfam-A.hmm were generated in February 2017.

Mapping and counting

The reads were mapped on the unigene set and plastidial genome of the corresponding species (GenBank accession numbers: MH590351 for EH, MH590354 for EP and MH590345 for CD; sequences submitted for review). For plastidial genes, contigs were mapped on plastidial genomes using STARlong (v2.5.2 with parameters –quantMode TranscriptomeSAM –alignIntronMax 1 –outFilterMismatchNmax 100 –seedSearchLmax 30 –seedSearchStartLmax 30 –seedPerReadNmax 100000 –seedPerWindowNmax 100 –alignTranscriptsPerReadNmax 100000 –alignTranscriptsPerWindowNmax 10000 –alignEndsType Local; Dobin *et al.*, 2013). These mapping contigs were removed from the unigene sets to avoid multimapping events. A GTF file corresponding to the non-plastidial contigs and the plastidial genome was created to perform the mapping of the reads with STAR (v2.5.2 with default parameters except –outFilterMultimapScoreRange 0 –alignIntronMax 1; Dobin *et al.*, 2013). The mapping rates ranged from 71 to 93% with an average of 78% for albinos and 90% for green samples. Reads mapping on exons were counted with featureCounts (v1.5.0,

© 2019 The Authors

parameters -M –s 2 –t exon –g gene_id; Liao *et al.*, 2014). Between 54 and 84% of the mapped reads were assigned with an average of 64% for albinos and 73% for green samples.

Orthology

To improve the annotation and allow the comparison of the transcriptome response to albinism in the three species, orthologues with rice (Oryza_sativa.IRGSP-1.0.pep.all), *Arabidopsis thaliana* (Arabidopsis_thaliana.TAIR10.pep.all) and *Phalaenopsis equestris* (GCF_001263595.1_ASM126359v1_protein) proteins were identified using OrthoFinder (v2.1.2; Emms and Kelly, 2015). 19 499 orthogroups out of 55 702 contained contigs of our three orchid species. They comprised 35 to 36% of all the contigs for each species, but between 69 and 94% of the reads with an average of 79% for the albinos and 90% for the green samples. For the transcriptome analysis, the count for an orthogroup was equal to the sum of counts of the contigs belonging to it.

Statistics

Only genes (orthogroups) for which read mapping was higher than one count per million in at least three samples were kept for further analysis. After normalization with the TMM method (Robinson *et al.*, 2010) to correct the library size effect, the counts were transformed with the vst method of the coseq package v1.2 (Rau and Maugis-Rabusseau, 2018). The QQ-plots showed that the resulting transformed counts fitted a normal distribution. As the samples were paired, the log2ratios albino/green calculated from the transformed counts was analyzed using the lmFit contrasts.fit and eBayes functions of the limma package v3.34.9 (Smyth, 2004). In our model, the log2ratio was expressed as a linear combination of a species effect and the p-values corresponding to the contrasts described in Data S1 were calculated. The distribution of the resulting p-values followed the quality criterion described by Rigaill *et al.* (2018). The Benjamini–Hochberg correction was used to control false discovery rate (FDR; Benjamini and Hochberg, 1995). We considered genes with an adjusted *P*-value ≤ 0.05 as being differentially expressed.

For metabolite abundance, log2 ratios between albinos and green counterparts were calculated for each pair. The same linear model as for gene expression analysis was fitted to each compound using functions lm and anova from R package stats v3.5.0 (R Core Team, 2018). The Benjamini–Hochberg correction was used to control FDR (Benjamini and Hochberg, 1995). We considered the metabolites with an adjusted *P*-value ≤ 0.05 as being differentially accumulated. Principal component analyzes shown in Figure S1 were carried out using the PCA function of the R package FactoMineR v1.41 (Husson *et al.*, 2010).

Vizualization

The 'omics results were further analyzed using Mapman v3.6.0RC1 (Thimm *et al.*, 2004). To use the *A. thaliana* mapping (Ath_AGI_LOCUS_TAIR10_Aug2012), only the orthogroups containing *A. thaliana* genes were kept. When several *A. thaliana* genes belonged to the same orthogroup, they were all given the ratio of this orthogroup. The final Mapman file contained values for 13 475 genes corresponding to 9081 orthogroups.

ACCESSION NUMBERS

Raw transcriptomic data are available at the NCBI Sequence Read Archive under the accession SRP140950. Raw metabolomic data are available upon request to the corresponding author.

ACKNOWLEDGEMENTS

We warmly thank the numerous field orchidologists who helped to collect the data, especially the Société Française d'Orchidophilie, Tela Botanica and the ophrys.bbactif community for field surveys, and Florent Baume, Laurence Blanchard, Joël Cottin, Adrien Chateignier, Jean-François Christians, Christiane Chynel, Alain Falvard, André Hasenfratz, Henri Mathé, Jean-Marc Moingeon, Franck Ramon, and Eva Schaller for field work. This study benefited from the financial support of the Fondation de France (Fondation Ars Cuttoli, granted to M-A Selosse) and the LabEx Saclay Plant Sciences-SPS (ANR-10-LABX-0040-SPS, granted to the IPS2).

CONFLICT OF INTEREST

The authors declare no conflict of interest.

SUPPORTING INFORMATION

Additional Supporting Information may be found in the online version of this article.

Figure S1. Principal component analyses (PCA) of transcriptomic (a–e) and metabolomic (f, g) data.

Figure S2. Nitrogen content of albino (A, pale colours) or green (G, deep colours) leaves of the different individuals sampled in the studied sites.

Figure S3. Overview of the average changes in the leaf transcriptome of white sectors compared with wild type photosynthetic sectors in the *Arabidopsis thaliana immutans* mutant, adapted from table S1 of Aluru *et al.* (2009).

Table S1. List of all metabolites detected by GC-MS analysis and corresponding changes between albino and green individuals (mean $\log_2$ ratio of the nine albino/green pairs studied).

Data S1. List of all orthogroups (OG) obtained in this work with corresponding fold changes of expression in the nine albino/green pairs ($\log_2$ ratio), mean fold changes and FDR.

REFERENCES

Abadie, J.-C., Püttsepp, Ü., Gebauer, G., Faccio, A., Bonfante, P. and Selosse, M.-A. (2006) *Cephalanthera longifolia* (Neottieae, Orchidaceae) is mixotrophic: a comparative study between green and nonphotosynthetic individuals. *Can. J. Bot.* **84**, 1462–1477.

Abadie, C., Lamothe-Sibold, M., Gilard, F. and Tcherkez, G. (2016) Isotopic evidence for nitrogen exchange between autotrophic and heterotrophic tissues in variegated leaves. *Funct. Plant Biol.* **43**, 298–306.

Aluru, M.R., Zola, J., Foudree, A. and Rodermel, S.R. (2009) Chloroplast photooxidation-induced transcriptome reprogramming in *Arabidopsis immutans* white leaf sectors. *Plant Physiol.* **150**, 904–923.

Araújo, W.L., Ishizaki, K., Nunes-Nesi, A. *et al.* (2010) Identification of the 2-hydroxyglutarate and isovaleryl-CoA dehydrogenases as alternative electron donors linking lysine catabolism to the electron transport chain of Arabidopsis mitochondria. *Plant Cell*, **22**, 1549–1563.

Araújo, W.L., Tohge, T., Ishizaki, K., Leaver, C.J. and Fernie, A.R. (2011) Protein degradation – an alternative respiratory substrate for stressed plants. *Trends Plant Sci.* **16**, 489–498.

Baena-González, E., Rolland, F., Thevelein, J.M. and Sheen, J. (2007) A central integrator of transcription networks in plant stress and energy signalling. *Nature*, **448**, 938–942.

Bellino, A., Alfani, A., Selosse, M.-A., Guerrieri, R., Borghetti, M. and Baldantoni, D. (2014) Nutritional regulation in mixotrophic plants: new insights from *Limodorum abortivum*. *Oecologia*, **175**, 875–885.

Benjamini, Y. and Hochberg, Y. (1995) Controlling the false discovery rate: a practical and powerful approach to multiple testing. *J. R. Stat. Soc. B*, **57**, 289–300.

Bidartondo, M.I., Burghardt, B., Gebauer, G., Bruns, T.D. and Read, D.J. (2004) Changing partners in the dark: isotopic and molecular evidence of

© 2019 The Authors
The Plant Journal © 2019 John Wiley & Sons Ltd,

ectomycorrhizal liaisons between forest orchids and trees. *Proc. Royal Soc. B*, **271**, 1799–1806.

Bolger, A.M., Lohse, M. and Usadel, B. (2014) Trimmomatic: a flexible trimmer for Illumina sequence data. *Bioinformatics*, **30**, 2114–2120.

Brouquisse, R., James, F., Pradet, A. and Raymond, P. (1992) Asparagine metabolism and nitrogen distribution during protein degradation in sugar-starved maize root tips. *Planta*, **188**, 384–395.

Brouquisse, R., Gaudillère, J.-P. and Raymond, P. (1998) Induction of a carbon-starvation-related proteolysis in whole maize plants submitted to light/dark cycles and to extended darkness. *Plant Physiol.* **117**, 1281–1291.

Buchanan-Wollaston, V., Page, T., Harrison, E. *et al.* (2005) Comparative transcriptome analysis reveals significant differences in gene expression and signalling pathways between developmental and dark/starvation-induced senescence in Arabidopsis. *Plant J.* **42**, 567–585.

Charlton, W.L., Johnson, B., Graham, I.A. and Baker, A. (2005) Non-coordinate expression of peroxisome biogenesis, β-oxidation and glyoxylate cycle genes in mature Arabidopsis plants. *Plant Cell Rep.* **23**, 647–653.

Chen, Z.-H., Walker, R.P., Acheson, R.M., Técsi, L.I., Wingler, A., Lea, P.J. and Leegood, R.C. (2000) Are isocitrate lyase and phosphoenolpyruvate carboxykinase involved in gluconeogenesis during senescence of barley leaves and cucumber cotyledons? *Plant Cell Physiol.* **41**, 960–967.

Contento, A.L., Kim, S.-J. and Bassham, D.C. (2004) Transcriptome profiling of the response of Arabidopsis suspension culture cells to suc starvation. *Plant Physiol.* **135**, 2330–2347.

Dearnaley, J.D.W., Martos, F. and Selosse, M.-A. (2012) Orchid mycorrhizas: molecular ecology, physiology, evolution and conservation aspects. In *Fungal Associations* (Hock, B., ed). Berlin, Heidelberg: Springer, pp. 207–230.

Dearnaley, J., Perotto, S. and Selosse, M.-A. (2016) Structure and development of orchid mycorrhizas. In *Molecular Mycorrhizal Symbiosis* (Martin, F., ed). Oxford: Wiley-Blackwell, pp. 63–86.

Diaz-Mendoza, M., Velasco-Arroyo, B., Santamaria, M.E., González-Melendi, P., Martinez, M. and Diaz, I. (2016) Plant senescence and proteolysis: two processes with one destiny. *Genet. Mol. Biol.* **39**, 329–338.

Dobin, A., Davis, C.A., Schlesinger, F., Drenkow, J., Zaleski, C., Jha, S., Batut, P., Chaisson, M. and Gingeras, T.R. (2013) STAR: ultrafast universal RNA-seq aligner. *Bioinformatics*, **29**, 15–21.

Emms, D.M. and Kelly, S. (2015) OrthoFinder: solving fundamental biases in whole genome comparisons dramatically improves orthogroup inference accuracy. *Genome Biol.* **16**, 157.

Feng, Y.-L., Wicke, S., Li, J.-W., Han, Y., Lin, C.-S., Li, D.-Z., Zhou, T.-T., Huang, W.-C., Huang, L.-Q. and Jin, X.-H. (2016) Lineage-specific reductions of plastid genomes in an orchid tribe with partially and fully mycoheterotrophic species. *Genome Biol. Evol.* **8**, 2164–2175.

Fiehn, O. (2006) Metabolite profiling in Arabidopsis. In *Arabidopsis Protocols* (Salinas, J. and Sanchez-Serrano, J.J., eds). Totowa, NJ: Humana Press, pp. 439–447.

Fiehn, O., Wohlgemuth, G., Scholz, M., Kind, T., Lee, D.Y., Lu, Y., Moon, S. and Nikolau, B. (2008) Quality control for plant metabolomics: reporting MSI-compliant studies. *Plant J.* **53**, 691–704.

Fochi, V., Chitarra, W., Kohler, A. *et al.* (2017) Fungal and plant gene expression in the *Tulasnella calospora–Serapias vomeracea* symbiosis provides clues about nitrogen pathways in orchid mycorrhizas. *New Phytol.* **213**, 365–379.

Garapati, P., Feil, R., Lunn, J.E., Van Dijck, P., Balazadeh, S. and Mueller-Roeber, B. (2015) Transcription factor Arabidopsis Activating Factor1 integrates carbon starvation responses with trehalose metabolism. *Plant Physiol.* **169**, 379–390.

Girlanda, M., Selosse, M.-A., Cafasso, D. *et al.* (2006) Inefficient photosynthesis in the Mediterranean orchid *Limodorum abortivum* is mirrored by specific association to ectomycorrhizal Russulaceae. *Mol. Ecol.* **15**, 491–504.

Gonneau, C., Jersáková, J., de Tredern, E., Till-Bottraud, I., Saarinen, K., Sauve, M., Roy, M., Hájek, T. and Selosse, M.-A. (2014) Photosynthesis in perennial mixotrophic *Epipactis* spp. (Orchidaceae) contributes more to shoot and fruit biomass than to hypogeous survival. *J. Ecol.* **102**, 1183–1194.

Haas, B.J., Papanicolaou, A., Yassour, M. *et al.* (2013) *De novo* transcript sequence reconstruction from RNA-seq using the Trinity platform for reference generation and analysis. *Nat. Protoc.* **8**, 1494–1512.

van der Heijden, M.G.A., Martin, F.M., Selosse, M.-A. and Sanders, I.R. (2015) Mycorrhizal ecology and evolution: the past, the present, and the future. *New Phytol.* **205**, 1406–1423.

Hildebrandt, T.M., Nunes-Nesi, A., Araújo, W.L. and Braun, H.-P. (2015) Amino acid catabolism in plants. *Mol. Plant*, **8**, 1563–1579.

Hirota, T., Izumi, M., Wada, S., Makino, A. and Ishida, H. (2018) Vacuolar protein degradation via autophagy provides substrates to amino acid catabolic pathways as an adaptive response to sugar starvation in *Arabidopsis thaliana*. *Plant Cell Physiol.* **59**, 1363–1376.

Husson, F., Lê, S. and Pagès, J. (2010). *Exploratory Multivariate Analysis by Example Using R*. Boca Raton, FL: Chapman & Hall.

Hynson, N.A., Madsen, T.P., Selosse, M.-A., Adam, I.K.U., Ogura-Tsujita, Y., Roy, M. and Gebauer, G. (2013) The physiological ecology of mycoheterotrophy. In *Mycoheterotrophy: The Biology of Plants Living on Fungi* (Merckx, V.S.F.T., ed). New York: Springer, pp. 297–342.

Jacquemyn, H., Waud, M., Brys, R., Lallemand, F., Courty, P.-E., Robionek, A. and Selosse, M.-A. (2017) Mycorrhizal associations and trophic modes in coexisting orchids: an ecological continuum between auto- and mixotrophy. *Front. Plant Sci.* **8**, 1497.

Julou, T., Burghardt, B., Gebauer, G., Berveiller, D., Damesin, C. and Selosse, M.-A. (2005) Mixotrophy in orchids: insights from a comparative study of green individuals and nonphotosynthetic individuals of *Cephalanthera damasonium*. *New Phytol.* **166**, 639–653.

Lallemand, F., Püttsepp, Ü., Lang, M., Luud, A., Courty, P.-E., Palancade, C. and Selosse, M.-A. (2017) Mixotrophy in Pyroleae (Ericaceae) from Estonian boreal forests does not vary with light or tissue age. *Ann. Bot.* **120**, 361–371.

Lallemand, F., Figura, T., Damesin, C., Fresneau, C., Griveau, C., Fontaine, N., Zeller, B. and Selosse, M.-A. (2019) Mixotrophic orchids do not use photosynthates for perennial underground organs. *New Phytol.* **221**, 12–17.

Lewis, L. (2015) Some observations on the nomenclature of achlorophyllous forms of *Epipactis purpurata E. helleborine* and *E. dunensis*. *J. Eur. Orch.* **47**, 111–122.

Liao, Y., Smyth, G.K. and Shi, W. (2014) featureCounts: an efficient general purpose program for assigning sequence reads to genomic features. *Bioinformatics*, **30**, 923–930.

Lunn, J.E., Delorge, I., Figueroa, C.M., Dijck, P.V. and Stitt, M. (2014) Trehalose metabolism in plants. *Plant J.* **79**, 544–567.

Merckx, V.S.F.T. (2013) Mycoheterotrophy: an introduction. In *Mycoheterotrophy: The Biology of Plants Living on Fungi* (Merckx, V.S.F.T., ed). New York: Springer, pp. 1–17.

Merckx, V.S.F.T., Freudenstein, J.V., Kissling, J., Christenhusz, M.J.M., Stotler, R.E., Crandall-Stotler, B., Wickett, N., Rudall, P.J., de Kamer, H.M. and Maas, P.J.M. (2013a) Taxonomy and classification. In *Mycoheterotrophy: The Biology of Plants Living on Fungi* (Merckx, V.S.F.T., ed). New York: Springer, pp. 19–101.

Merckx, V.S.F.T., Mennes, C.B., Peay, K.G. and Geml, J. (2013b) Evolution and diversification. In *Mycoheterotrophy: The Biology of Plants Living on Fungi* (Merckx, V.S.F.T., ed). New York: Springer, pp. 215–244.

Nakasugi, K., Crowhurst, R., Bally, J. and Waterhouse, P. (2014) Combining transcriptome assemblies from multiple *de novo* assemblers in the allotetraploid plant *Nicotiana benthamiana*. *PLoS ONE*, **9**, e91776.

Ng, C.K.Y. and Hew, C.S. (1996) Pathway of phloem loading in the C3 tropical orchid hybrid *Oncidium goldiana*. *J. Exp. Bot.* **47**, 1935–1939.

Pao, S.S., Paulsen, I.T. and Saier, M.H. (1998) Major facilitator superfamily. *Microbiol. Mol. Biol. Rev.* **62**, 1–34.

Pistelli, L., Perata, P. and Alpi, A. (1992) Effect of leaf senescence on glyoxylate cycle enzyme activities. *Funct. Plant Biol.* **19**, 723–729.

Preiss, K., Adam, I.K.U. and Gebauer, G. (2010) Irradiance governs exploitation of fungi: fine-tuning of carbon gain by two partially myco-heterotrophic orchids. *Proc. Royal. Soc. B*, **277**, 1333–1336.

Press, M.C., Smith, S. and Stewart, G.R. (1991) Carbon acquisition and assimilation in parasitic plants. *Funct. Ecol.* **5**, 278–283.

R Core Team (2018). *R: A Language and Environment for Statistical Computing*. Vienna: R Foundation for Statistical Computing.

Rau, A. and Maugis-Rabusseau, C. (2018) Transformation and model choice for RNA-seq co-expression analysis. *Brief. Bioinform.* **19**, 425–436.

Rigaill, G., Balzergue, S., Brunaud, V. *et al.* (2018) Synthetic data sets for the identification of key ingredients for RNA-seq differential analysis. *Brief. Bioinform.* **19**, 65–76.

© 2019 The Authors

Roberts, W.R. and Roalson, E.H. (2017) Comparative transcriptome analyses of flower development in four species of *Achimenes* (Gesneriaceae). *BMC Genomics*, **18**, 240.

Robinson, M.D., McCarthy, D.J. and Smyth, G.K. (2010) edgeR: a Bioconductor package for differential expression analysis of digital gene expression data. *Bioinformatics*, **26**, 139–140.

Roy, M., Gonneau, C., Rocheteau, A., Berveiller, D., Thomas, J.-C., Damesin, C. and Selosse, M.-A. (2013) Why do mixotrophic plants stay green? A comparison between green and achlorophyllous orchid individuals *in situ*. *Ecol. Monogr.* **83**, 95–117.

Sakamoto, Y., Ogura-Tsujita, Y., Ito, K., Suetsugu, K., Yokoyama, J., Yamazaki, J., Yukawa, T. and Maki, M. (2016) The tiny-leaved orchid *Cephalanthera subaphylla* obtains most of its carbon via mycoheterotrophy. *J. Plant. Res.* **129**, 1013–1020.

Salmia, A. (1989) General morphology and anatomy of chlorophyll-free and green forms of *Epipactis helleborine* (Orchidaceae). *Ann. Bot. Fennici*, **26**, 95–105.

Schulz, M.H., Zerbino, D.R., Vingron, M. and Birney, E. (2012) Oases: robust *de novo* RNA-seq assembly across the dynamic range of expression levels. *Bioinformatics*, **28**, 1086–1092.

Selosse, M.-A. and Martos, F. (2014) Do chlorophyllous orchids heterotrophically use mycorrhizal fungal carbon? *Trends Plant Sci.* **19**, 683–685.

Selosse, M.-A. and Roy, M. (2009) Green plants that feed on fungi: facts and questions about mixotrophy. *Trends Plant Sci.* **14**, 64–70.

Selosse, M.-A., Faccio, A., Scappaticci, G. and Bonfante, P. (2004) Chlorophyllous and achlorophyllous specimens of *Epipactis microphylla* (Neottieae, Orchidaceae) are associated with ectomycorrhizal septomycetes, including truffles. *Microb. Ecol.* **47**, 416–426.

Selosse, M.-A., Charpin, M. and Not, F. (2017) Mixotrophy everywhere on land and in water: the grand écart hypothesis. *Ecol. Lett.* **20**, 246–263.

Shefferson, R.P., Roy, M., Püttsepp, Ü. and Selosse, M.-A. (2016) Demographic shifts related to mycoheterotrophy and their fitness impacts in two *Cephalanthera* species. *Ecology*, **97**, 1452–1462.

Smith, S.E. and Read, D.J. (2008) *Mycorrhizal Symbiosis*. London: Academic Press.

Smith, S.E. and Smith, F.A. (1973) Uptake of glucose, trehalose and mannitol by leaf slices of the orchid *Bletilla hyacinthina*. *New Phytol.* **72**, 957–964.

Smyth, G. K. (2004). Linear models and empirical Bayes methods for assessing differential expression in microarray experiments. *Stat. Appl. Genet. Mol. Biol.* **3**, Article3.

Suetsugu, K., Yamato, M., Miura, C., Yamaguchi, K., Takahashi, K., Ida, Y., Shigenobu, S. and Kaminaka, H. (2017) Comparison of green and albino individuals of the partially mycoheterotrophic orchid *Epipactis helleborine* on molecular identities of mycorrhizal fungi, nutritional modes and gene expression in mycorrhizal roots. *Mol. Ecol.* **26**, 1652–1669.

Suetsugu, K., Ohta, T. and Tayasu, I. (2018) Partial mycoheterotrophy in the leafless orchid *Cymbidium macrorhizon*. *Am. J. Bot.* **105**, 1595–1600.

Tcherkez, G., Guérard, F., Gilard, F., Lamothe, M., Mauve, C., Gout, E. and Bligny, R. (2012) Metabolomic characterisation of the functional division of nitrogen metabolism in variegated leaves. *Funct. Plant Biol.* **39**, 959–967.

Těšitel, J., Těšitelová, T., Minasiewicz, J. and Selosse, M.-A. (2018) Mixotrophy in land plants: why to stay green? *Trends Plant Sci.* **23**, 656–659.

Thimm, O., Bläsing, O., Gibon, Y., Nagel, A., Meyer, S., Krüger, P., Selbig, J., Müller, L.A., Rhee, S.Y. and Stitt, M. (2004) Mapman: a user-driven tool to display genomics data sets onto diagrams of metabolic pathways and other biological processes. *Plant J.* **37**, 914–939.

Tranchida-Lombardo, V., Roy, M., Bugot, E., Santoro, G., Püttsepp, Ü., Selosse, M. and Cozzolino, S. (2010) Spatial repartition and genetic relationship of green and albino individuals in mixed populations of *Cephalanthera* orchids. *Plant Biol.* **12**, 659–667.

Üstün, S., Hafrén, A. and Hofius, D. (2017) Autophagy as a mediator of life and death in plants. *Curr. Opin. Plant Biol.* **40**, 122–130.

Waterhouse, R.M., Seppey, M., Simão, F.A., Manni, M., Ioannidis, P., Klioutchnikov, G., Kriventseva, E.V. and Zdobnov, E.M. (2018) BUSCO applications from quality assessments to gene prediction and phylogenomics. *Mol. Biol. Evol.* **35**, 543–548.

Waterman, R.J., Klooster, M.R., Hentrich, H. and Bidartondo, M.I. (2013) Species interactions of mycoheterotrophic plants: specialization and its potential consequences. In *Mycoheterotrophy: The Biology of Plants Living on Fungi* (Merckx, V.S.F.T., ed). New York: Springer, pp. 267–296.

Zrenner, R., Stitt, M., Sonnewald, U. and Boldt, R. (2006) Pyrimidine and purine biosynthesis and degradation in plants. *Annu. Rev. Plant Biol.* **57**, 805–836.

© 2019 The Authors
The Plant Journal © 2019 John Wiley & Sons Ltd,